Superconductivity in 4 Angstrom Single-Walled Carbon Nanotubes

Z. K. Tang, Lingyun Zhang, N. Wang, X. X. Zhang, G. H. Wen, G. D. Li, J. N. Wang, C. T. Chan, Ping Sheng*

Investigation of the magnetic and transport properties of single-walled small-diameter carbon nanotubes embedded in a zeolite matrix revealed that at temperatures below 20 kelvin, 4 angstrom tubes exhibit superconducting behavior manifest as an anisotropic Meissner effect, with a superconducting gap and fluctuation supercurrent. The measured superconducting characteristics display smooth temperature variations owing to one-dimensional fluctuations, with a mean-field superconducting transition temperature of 15 kelvin. Statistical mechanic calculations based on the Ginzburg-Landau free-energy functional yield predictions that are in excellent agreement with the experiments.

Superconductivity in organic conductors was first reported in pressurized quasi–one-dimensional (1D) tetramethyltetraselenafulvalene (TMTSF) Bechgaard salt $(TMTSF)_2PF_6$ (*1*, *2*). After the discovery of the fullerenes, superconductivity was observed in alkali metal–doped crystals of C_{60} (*3*, *4*). More recently, hole-doped C_{60} crystals were shown to be superconducting at 52 K (*5*). Carbon nanotubes have also been observed to pass supercurrents between superconducting leads, owing to the proximity effect (*6*). In view of these findings, a natural question is: Can pure carbon be superconducting in any of its many forms (*7*)?

We report the observation of 1D superconductivity in single-walled 4 Å carbon nanotubes, fabricated by pyrolyzing tripropylamine in the channels of the zeolite crystals $AlPO_4$-5 (AFI) (*8*). These nanotubes have been observed directly by transmission electron microscopy (*9*), as well as indirectly by diffuse x-ray scattering (*10*) and micro-Raman measurements of the nanotube breathing mode (*11*). The data consistently indicate a nanotube diameter of 4.2 ± 0.2 Å, probably at or close to the theoretical limit. Because the single-walled nanotubes (SWNTs) are formed inside the ordered channels of AFI, they are highly aligned and uniform in size, and because the SWNTs are isolated from each other, they constitute an almost ideal 1D system. The data (*12*) are consistent with the manifestations of a 1D BCS (phonon-mediated) superconductor with a mean-field T_c^o = 15 K and (zero temperature) coherence length $\xi_o \approx 4.2$ nm along the tube direction.

Temperature-dependent magnetic susceptibilities for all of the samples were obtained with the Quantum Design superconducting quantum interference device magnetometer (MPMS-5S) equipped with a 5-T magnet. Two samples were measured. Sample A, used for background deduction, consists of columnar zeolite crystallites about 300 μm long and 100 μm in diameter. Sample B is composed of similar crystallites but with nanotubes formed inside their channels. For both samples, the c axes of the crystallites were aligned by hand to form a parallel array and fixed. It is estimated that there is a maximum error of ±10° in the alignment. Both samples were dried and weighed.

Both samples were characterized magnetically by the same procedure. The samples were first cooled to 1.8 K, and then a magnetic field was applied. The magnetization was measured as a function of temperature while warming from 1.8 to 50 K. The measurements were repeated by cooling with the applied field. At each temperature, the magnetization was measured after the temperature was stabilized for 60 s. The results of zero-field–cooled and field-cooled measurements are almost identical (Fig. 1) (*13*). The measured magnetization of sample A is isotropic with respect to the field orientation and exhibits a small, temperature-independent diamagnetic component plus a paramagnetic component that follows an excellent Curie-Weiss law (Fig. 1, inset).

For sample B, the measured magnetization is anisotropic with respect to the field orientation (*14*). After a simple deduction of the pure zeolite crystallite contribution (using the data obtained from sample A) and normalizing to the nanotube volume, the temperature dependence of the SWNTs' magnetic susceptibility is shown for five values of applied field perpendicular to the c axes (Fig. 1). A strongly temperature-dependent diamagnetism is seen below 10 K, at 0.02- or 0.2-T applied field. The magnitude of the susceptibility decreases monotonically with increasing field and is very small at 5 T. The result is in quantitative agreement with the Meissner effect of 1D fluctuation superconductivity, shown below. The susceptibility of the parallel field case is one order of magnitude less, within the error caused by the crystallites' misalignment and consistent with the observation that there is no Meissner effect under a parallel field for 1D systems (*15*).

The superconductivity of 1D systems can be described by the Ginzburg-Landau (GL) free-energy (line) density (*16*, *17*)

$$f[\psi(x)] = \frac{1}{2m^*}\left|\left(\frac{\hbar}{i}\vec{\Delta} + \frac{2e\vec{A}}{c}\right)\psi(x)\right|^2 + \alpha_0(T - T_c^o)|\psi(x)|^2 + \gamma|\psi(x)|^4 + \frac{HB}{8\pi}\Sigma \quad (1)$$

where x is the spatial coordinate along nanotube's length direction, $\psi(x)$ is the (complex) GL wavefunction, m^* is twice the electron effective mass, c is the speed of light, $\hbar$ is Planck's constant, e is the electronic charge, $\vec{A}$ is the vector potential of the applied field, T_c^o is the mean field transition temperature, and α_o and γ are parameters related to the coherence length $\xi^2(T) = \xi_o^2/(1 - t)$, with $\xi_o^2 = \hbar^2/(2m^*\alpha_o T_c^o)$ and $t = T/T_c^o$, and the magnetic penetration length λ. The last term of Eq. 1 represents the magnetic-field energy, with Σ the cross-sectional area of the sample. From Eq. 1, the superconducting state is favored locally at $T \leq T_c^o$. However, it is characteristic of 1D systems that the diverging long-wavelength fluctuation amplitudes of $\psi(x)$ (at any finite transition temperature), when considered together with the density of states, means that macroscopically, the superconducting transition can only be achieved at $T = 0$ K. Between $T \approx T_c^o$ and $T = 0$ the superconductivity is not totally destroyed but can manifest superconducting behavior strongly modified by the fluctuation effects. To calculate such behavior statistically, we use the path-integral formulation of the partition function Z:

$$Z = \int D[\psi(x)]\exp\{-\beta F_{GL}[\psi(x)]\} \quad (2)$$

where $\beta = 1/kT$, k is the Boltzmann constant, and $F_{GL}[\psi(x)] = \int f[\psi(x)]dx$ is the GL free energy (functional). The total free energy of the system is $F = -kT \ln Z$. For a perpendicular applied magnetic field $\vec{B}$, $\vec{A} = Bx\hat{j}$, with $\hat{j}$ the unit vector along the y direction. The magnetic susceptibility is given by $\chi = -\partial^2 F/\partial B^2$.

To apply the 1D GL formalism to our system, we wish to specify the 1D character-

Department of Physics and Institute of Nano Science and Technology, Hong Kong University of Science and Technology, Clear Water Bay, Kowloon, Hong Kong, China.

*To whom correspondence should be addressed. E-mail: phsheng@ust.hk

ization to mean the essential absence of interaction between the SWNTs, so that the statistical fluctuation effects formulated in Eqs. 1 and 2 are fully manifest. Owing to imperfections, the superconductivity in SWNTs probably exists in segments. Therefore, one has to take into account the finite diameter of the nanotubes to invoke elongated current loops associated with the Meissner effect. That means deviation from the mathematical 1D formulation as implied by $\psi(x)$ in Eq. 1. For the parallel field case, the associated current is circumferential. However, because the SWNTs are insulating in the transverse direction (*18*), we expect no Meissner effect. In addition, because the susceptibility of each AFI crystallite (containing the SWNTs) is very small, so that $\mu \cong 1$, therefore (within the temperature range of consideration) the magnetic field inside the crystallites, as seen by the SWNTs, is essentially the same as the externally applied field B_a (*19*).

We have carried out Monte Carlo calculations of the path integrals involved in the susceptibility expression using the Metropolis algorithm (*20*, *21*) (Fig. 1). Apart from a normalizing constant, quantitative agreement is seen for the temperature and magnetic-field variations with parameter values (*22*) T_c^o = 15 K, $\alpha_o T_c^o$ = 6 meV, and γ = 1.3 meV Å. The effective mass obtained is m^* = 0.36m (where m is the free electron mass), which is in reasonable agreement with that for the metallic (5,0) nanotubes, 0.24m, calculated from the local density approximation (LDA) scheme (*23*). The (zero temperature) magnetic penetration length can also be evaluated from the value of γ to yield $\lambda_o = \sqrt{m^* c^2 \gamma \pi r_o^2 / 16\pi e^2 \alpha_o T_c^o}$ = 39 Å, where r_o = 2.1 Å is the nanotube radius. Because $r_o \ll \lambda_o$, 100% Meissner effect cannot be achieved in the SWNTs.

The Meissner effect associated with 1D superconductivity differs substantially from the conventional behavior of an abrupt susceptibility jump at T_c^o. Here, the dominance of 1D fluctuations means that the critical phenomenon around T_c^o is replaced by smooth temperature and magnetic-field variations. Because all of these can be accurately captured by the (path integral calculations of) 1D wave functionals, the SWNTs should be well insulated from each other, in contrast to the superconductivity in many quasi-1D systems (*1*, *2*), where even weak interchain interaction can restore the basic (anisotropic) 3D character of superconductivity (*24*).

To measure the electric transport characteristics, we first mounted one AFI zeolite crystallite containing the SWNTs in an insulating matrix (glass or ceramic). The matrix was then sectioned into thin foil by mechanical polishing. The normal direction of the foil surface was precisely controlled so that the SWNT-containing AFI crystal was sectioned simultaneously with its channels perpendicular to the foil surface. The lengths of SWNTs sectioned were determined by the foil thickness. Chemical etching (with 18% HCl) was carried out to remove a layer of AFI damaged by polishing. By this etching process, SWNTs emerged out of the AFI surfaces because the HCl etched only the AFI. The thickness of the AFI crystallite (the length of SWNTs) can be controlled within the range of 100 to 5 μm. Pt electrodes were then coated on both sides of the foil by focused ion beam (FIB) deposition. Because AFI zeolite is insulating, the conductance of the sample directly reflects the conductance of the SWNTs. Linear current-voltage (I-V) relations, in the temperature range of 30 K < T < 300 K, indicate good ohmic contact between the electrodes and the nanotubes. The lower bound of nanotube conductivity at room temperature, obtained by assuming that every AFI channel is filled with a nanotube bridging the two electrodes, is about 10 $\text{ohm}^{-1}\ \text{cm}^{-1}$, or ~1% of the graphite conductivity. From 30 K to room temperature, the temperature dependence of the conductivity σ displays a $\ln\sigma \propto -1/\sqrt{T}$ behavior, characteristic of 1D hopping conduction (*25*). These data indicate the existence of potential

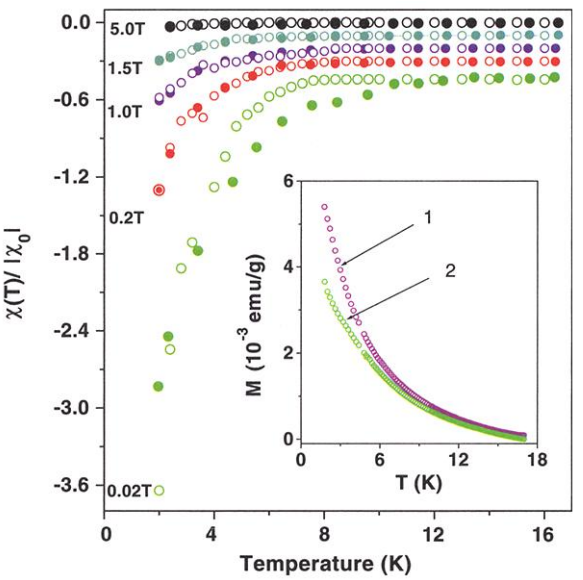

Fig. 1. Normalized magnetic susceptibility of the SWNTs plotted as a function of temperature for five values of the magnetic field. The curves are displaced vertically for clarity. Values shown are for theory (open symbols) and experiment (filled symbols). χ_o denotes the value of the susceptibility at T = 1.6 K and magnetic field = 0.2 T. The experimental value of χ_o, when normalized to the volume of the SWNTs, is −0.015 (in units where B = 0 denotes χ = −1). The scatter in the theory points reflects statistical fluctuations inherent in the Monte Carlo calculations. **(Inset)** Temperature dependence of magnetization density for zeolite AFI crystallites (curve 1) and for AFI crystallites with SWNTs in their channels (curve 2). Both curves are measured at 2000 Oe.

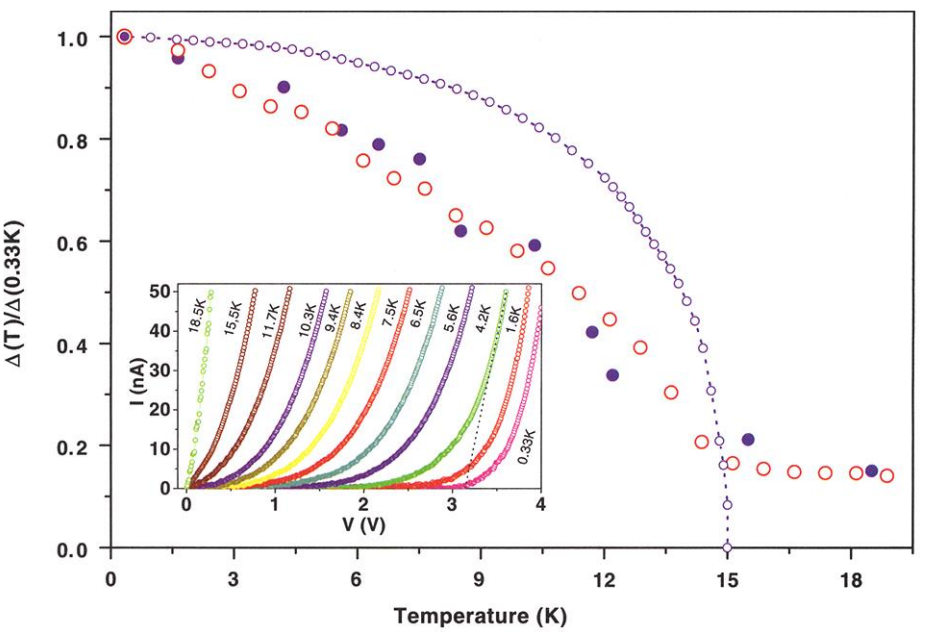

Fig. 2. Temperature dependence of the gap, normalized to its value at 0.33 K. Values shown are for theory (open symbols) and experiment (filled symbols). ○–○ denotes the BCS gap. **(Inset)** The I-V curves at various temperatures. The dashed line at 4.2 K illustrates the extrapolation from the high field. To a reasonable approximation, the intercept is proportional to the gap magnitude.

fluctuations caused by imperfections along the length of the nanotubes. Hence only the normal current, as opposed to a supercurrent, is expected for macroscopic samples because the superconductivity is punctuated by many potential barriers, at least one of which may destroy coherent tunneling. Indeed, at $T < 20$ K, the I-V curves shown in the inset to Fig. 2 indicate the disappearance of charge carriers with the opening of a gap at the Fermi level. This behavior is reproducible not only on the same sample, but also on different samples. By extrapolating from the high-field asymptote back to the horizontal axis, shown by the dashed line for the 4.2 K curve, the V intercept is indicative of the magnitude of the gap (*26*). The temperature variation of the gap is summarized in Fig. 2. The theoretical prediction for the temperature variation of the 1D superconducting gap is calculated (by the Monte Carlo approach) from the ensemble average of $|\psi(x)|$ (which is proportional to the gap):

$$\langle|\psi(x)|\rangle = \frac{1}{Z}\int D[\psi(x)] \times |\psi(x)|\exp\{-\beta F_{GL}[\psi(x)]\} \quad (3)$$

The excellent agreement between theory and experiment (Fig. 2), with no adjustable parameters, strongly supports the model of 1D superconductivity in SWNTs and is consistent with the magnetic data on the Meissner effect. Here, the 1D fluctuations are seen to substantially alter the temperature variation from its mean field behavior at $T \leq T_c^o$ and give rise to some finite level of $\langle|\psi(x)|\rangle$ at $T \geq T_c^o$.

To observe the supercurrents, it is necessary to fabricate thin samples to ensure that there is no potential barrier within the length of the SWNTs. This is done by further reducing the thickness of the AFI foil to about 50 nm by argon ion milling both sides of the foil. Such a thin foil is translucent, as observed by scanning electron microscopy (SEM) (Fig. 3A). After etching (with HCl) and cleaning (with distilled water) of the foil, Pt electrodes were made on both sides of the foil by FIB deposition. The size and location of the Pt electrodes were precisely controlled by FIB, ensuring good contact between the electrodes and the ends of SWNTs. Figure 3B shows the sideways geometry of the sample. The foil is thinnest close to the edge of a hole in the foil, with a thickness of ~50 nm, and becomes progressively thicker away from the edge. The top and bottom electrodes thus measure, in parallel, electrical transport by both short and long SWNTs. We first measured the electrical conductance of the sample by applying a fixed voltage across the sample and monitoring the current J as a function of temperature. To obtain measurable currents above the noise level, we applied 1 V (corresponding to an electric field of $E \approx 2 \times 10^5$ V/cm at the thinnest section) in all the measurements. The measured conductance displays a minimum at about 10 K (Fig. 4 inset, curve 1), below which the conductance increases as the temperature decreases (i.e., exhibits the metallic behavior). This behavior is believed to arise from the thinnest section of the sample, because the conductance at the thicker section should decrease markedly at low temperatures; hence, most of the current should pass through the thinnest part. To verify this proposition, we used argon ion milling to remove the tips of the top and bottom electrodes, as well as a portion (~0.1 μm^2) of the thinnest part of the sample (Fig. 3B). The altered sample displays monotonically decreasing conductance down to the lowest temperatures (Fig. 4 inset, curve 2). Moreover, the difference between the first measured conductance G_1 ($=J_1/V$) and the second measured conductance G_2 ($=J_2/V$), $\Delta G = G_1 - G_2$, is attributable to the removed (the thinnest) part of the sample. When normalized to a single SWNT, the conductivity lower bound at 2 K, for the thinnest section of the sample, is ~100 ohm^{-1} cm^{-1}. In Fig. 4, the ΔG (at 1 V, or an electric field $\approx 2 \times 10^5$ V/cm) is plotted as a function of temperature (*27*). To explain this conductance behavior (at $T \sim 15$ K or less), we calculated the ensemble-averaged current using the Monte Carlo approach,

$$\langle J(x)\rangle_E = \frac{1}{Z}\int D[\psi(x)] \times J(x)\exp\{-\beta F'_{GL}[\psi(x)]\} \quad (4)$$

where $J(x) = (2e\hbar/m^*)\mathrm{Im}\{\psi^*(x)[d\psi(x)dx]\}$ is the current expression, with $\psi^*(x)$ the complex conjugate of $\psi(x)$, and Im{ } means taking the imaginary part. Here

$$F'_{GL} = F_{GL} - \int dx e E x |\psi(x)|^2 \quad (5)$$

The calculated (normalized) conductivity J/E (evaluated at the experimental $E_{exp} \approx 2 \times 10^5$ V/cm) is in excellent agreement with the experiment (Fig. 4), again with no adjustable parameters. The sample at $T \leq T_c^o$ cannot be at zero resistance (even without potential barriers) because at any given instant there is always some probability that fluctuations would locally drive the superconducting state to the normal state. In a 1D system, any normal segment is in series with the rest of the sample, and hence there is always a finite

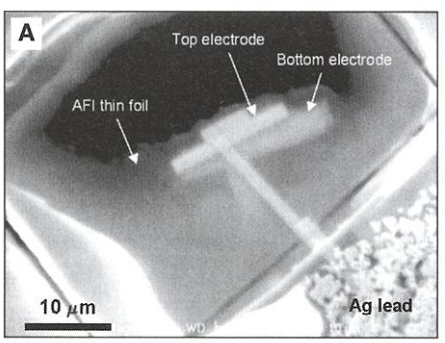

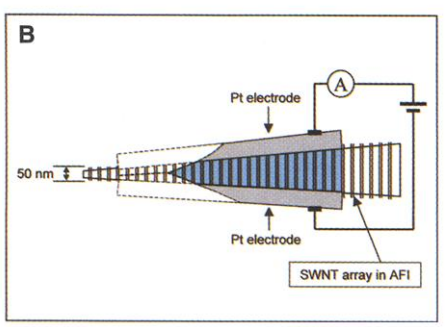

Fig. 3. (**A**) Scanning electron micrograph of the sample after thinning by argon milling. The dark region is a hole in the foil. Because the foil is translucent in its thinnest part, the bottom electrode is dimly visible. (**B**) A diagram of the sample. Shading indicates the part of the sample after the tip has been removed.

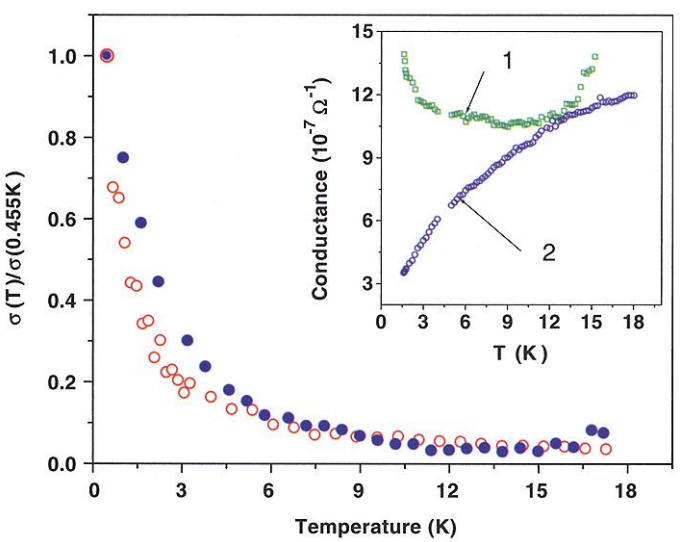

Fig. 4. The normalized conductivity plotted as a function of temperature for the thinnest part of the sample shown in Fig. 3, ~50 nm thick. Experimental values (filled circles) and the theoretical predictions for the fluctuation supercurrent (open circles) are shown. The estimate for the lower bound of nanotube conducitivity σ(0.445 K) is 320 ohm^{-1} cm^{-1}. (**Inset**) The measured sample conductances, labeled as 1 and 2 in the text.

resistance at finite temperatures. Because such a probability decreases with temperature, the fluctuation supercurrent, and hence the conductance, increases. Zero resistance is reached only at $T = 0$ K.

Note added in proof: After the submission of this manuscript, superconductivity in ropes of nanotubes was reported (*28*).

References and Notes

1. D. Jerome, A. Mazaud, M. Ribault, K. Bechgaard, *J. Phys. (Paris) Lett.* **41**, L95 (1980).
2. T. Ishiguro, K. Yamaji, G. Saito, *Organic Superconductors* (Springer, Berlin, ed. 2, 1998).
3. A. F. Hebard *et al.*, *Nature* **350**, 600 (1991).
4. K. Tanigaki *et al.*, *Nature* **352**, 222 (1991).
5. J. H. Schon, Ch. Kloc, B. Batlogg, *Nature* **408**, 549 (2000).
6. A. Yu. Kasumov *et al.*, *Science* **284**, 1508 (1999).
7. The possibility of superconductivity in carbon nanotubes has been predicted, with a transition temperature that increases with decreasing diameter owing to the enhanced electron-phonon interaction. See (*29*).
8. Z. K. Tang, H. D. Sun, J. N. Wang, J. Chen, G. D. Li, *Appl. Phys. Lett.* **73**, 2287 (1998).
9. N. Wang, Z. K. Tang, G. D. Li, J. S. Chen, *Nature* **408**, 50 (2000).
10. P. Launois *et al.*, *Solid State Commun.* **116** (2), 99 (2000).
11. H. D. Sun, Z. K. Tang, J. Chen, G. D. Li, *Appl. Phys.* A **69**, 381 (1999).
12. Magnetic and electrical transport measurements were reproducible on the same sample over a period of a few months, indicating that the nanotubes inside the AFI channels were stable.
13. There is some evidence that at very small magnetic fields there is a difference between the field-cooled and zero-field–cooled data. However, the measured magnetization signals are too small to be definitive. At 0.2 T, the measured magnetization is substantially above the noise level.
14. The anisotropy in the measured magnetic data suggests that the data are unlikely to arise from random magnetic impurities, because such an effect should be isotropic with respect to the field orientation.
15. For an infinite tube with a radius R, the Meissner effect under a parallel field requires a circumferential surface current. However, quantization of electronic motion in the circumferential direction means that the electron energy levels are discrete, with an average level separation that varies as $1/R^2$. Thus, as R diminishes to zero, the 1D system is necessarily insulating in the transverse direction, i.e., there is no circumferential current.
16. V. L. Ginzburg, L. D. Landau, *Zh. Eksp. Teor. Fiz.* **20**, 1064 (1950).
17. P. G. de Gennes, *Superconductivity of Metals and Alloys* (Benjamin, New York, 1966), p. 171.
18. For polarization transverse to the SWNTs, the sample is transparent to visible light, whereas for polarization parallel to the SWNTs, the sample is opaque. This is an indication that the sample is insulating in the transverse direction.
19. Because the superconducting region may be as large as 50 nm (indicated by the supercurrent experiment), the charging energy is small. Thus, the quantum effect would apply only at very low temperatures.
20. N. Metropolis, A. W. Rosenbluth, M. N. Rosenbluth, A. H. Teller, E. Teller, *J. Chem. Phys.* **21**, 1087 (1953).
21. K. Binder, Ed., *Monte Carlo Methods in Statistical Physics* (Springer-Verlag, Berlin, 1979), p. 1. The calculations are carried out by starting at $T = 30$ K with an initial Gaussian wavefunction whose width is proportional to $1/B$. Simulated annealing is then carried out by cooling at 0.04 K intervals, and at each temperature, 10^7 to 10^8 Metropolis steps were carried out. At each Metropolis step, a random complex number ($\rho \cos\theta$, $\rho \sin\theta$) was generated, with $0 < \rho \leq 1$ and $-\pi > \theta \leq \pi$, as a potential additive change to $\psi(x)$. Spatial discretization is at the level of 16 points per coherence length, and 6 points were used to calculate the numerical derivative to third-order accuracy. The length of the sample used is $60\xi_o$ to $250\xi_o$. Down to $T \approx 0.1$ K, the finite size effect is within the statistical fluctuations of the calculated results. Meissner effect calculations were carried out by considering a 4 Å strip. Hence, in Eq. 1 the $\psi(x)$ is replaced by $\psi(x,y)$.
22. The temperature and magnetic-field variations of the magnetic susceptibility represent a reasonably constraining set of conditions for the determination of the parameter values. For example, α_o enters in both the temperature and magnetic-field variations, and $\alpha_o T_c^o$ is the energy unit in the GL theory. The error in the parameter values is estimated to be $\sim \pm 10\%$.
23. We have carried out LDA calculations on the (5,0), (3,3), and (4,2) nanotubes. Diameters are found to be 4.04, 4.20, and 4.27 Å, respectively. (4,2) is a semiconductor, whereas (5,0) and (3,3) are metallic, and the density of states at the Fermi level is 0.21 and 0.06 states per eV per C atom, respectively. The effective band mass of (3,3) is at least one order of magnitude larger than that for the (5,0). The metallicity of (5,0) is due to strong σ-π mixing induced by the large curvature of the tube. Large-scale LDA calculation has also been carried out in regard to the Peierls transition in the nanotubes. The negative results indicate that the transition temperature could be very low.
24. It also implies weak interaction between the nanotubes and the walls of the zeolite channels, because with a zeolite thickness of only 7.4 Å between the nanotubes, any interaction between the nanotubes and the zeolite channel walls would translate into interaction between the nanotubes.
25. Z. K. Tang, H. D. Sun, J. N. Wang, *Physica* B **279**, 200 (2000).
26. By estimating the average superconducting segment as 0.1-μm long and taking the low-temperature intercept as 4 V, our sample (with a thickness of 100 μm) has about 1000 superconducting segments, separated by potential barriers. That translates into a measured low-temperature gap width of ~4 meV, which is in good agreement with the BCS formula of $2\Delta(0) = 3.6kT_c^o \approx 4$ meV.
27. ΔG increases with temperature for $T > 15$ K. Such nonmetallic behavior is not unusual for a 1D Luttinger liquid.
28. M. Kociak *et al.*, *Phys. Rev. Lett.* **86**, 2416 (2001).
29. L. X. Benedict, V. H. Crespi, S. G. Louie, M. L. Cohen, *Phys. Rev.* B **52**, 14935 (1995).

30. We thank K. Y. Lai for technical assistance with the FIB system and T. K. Ng, P. Yu, and L. Chang for helpful comments. Partially supported by University Grants Committee of Hong Kong grants HIA98/99.SC01 and DAG 00/01.SC27, Research Grants Council grant HKUST 6152/99P, and SAE Company grant SAE 95/96.SC01.

7 March 2001; accepted 17 May 2001

Construction Principles of "Hyparenes": Families of Molecules with Planar Pentacoordinate Carbons

Zhi-Xiang Wang* and Paul von Ragué Schleyer†

Density-functional theory calculations predict that three borocarbon units with planar pentacoordinate carbons $-C_3B_3-$, $-C_2B_4-$, and $-CB_5-$, can replace the $-(CH)_3-$ subunits in aromatic or even in antiaromatic hydrocarbons to construct "hyparenes" (families of molecules with planar pentacoordinate carbons). These borocarbon units contribute two, one, and zero electrons, respectively, to the parent pi system. Depending on the choice of these units, the hyparenes (judging from computed proton and nucleus-independent chemical shifts), can maintain or can interconvert the aromatic or antiaromatic character of the parent compounds. The hyparenes are low-lying local minima with normal carbon-boron, boron-boron, and carbon-carbon bond lengths. The multicenter bonding in the hyparenes involves contributions of partial sigma and partial pi bonds to the planar pentacoordinate carbons; the octet rule is not violated. Borocarbon species, for which there is some mass spectrometric evidence, might be observed and identified, for example, in matrix isolation by vibrational spectroscopy.

The principles of the mechanical molecular models for hydrocarbons, still widely used to visualize organic structures, have remained essentially unchanged since van't Hoff introduced folded paper tetrahedra (*1*, *2*) as the first three-dimensional representation. Placed corner-to-corner, two of these methane tetrahedra represent ethane. Two tetrahedra joined edge-to-edge have four coplanar vertices and model ethylene. Similarly, an acetylene model results from a face-to-face arrangement.

Here we predict simple structural groupings, based on planar pentacoordinate carbons (ppC) [$-C_3B_3-$ (type **A**), $-C_2B_4-$ (type **B**), and $-CB_5-$ (type **C**)] (Fig. 1),

Center for Computational Quantum Chemistry, Computational Chemistry Annex, University of Georgia, Athens, GA 30602–2525, USA.

*Permanent address: Graduate School at Beijing, University of Science and Technology of China, Academia, Sinica, Beijing 10039, People's Republic of China.

†To whom correspondence should be addressed. E-mail: schleyer@chem.uga.edu